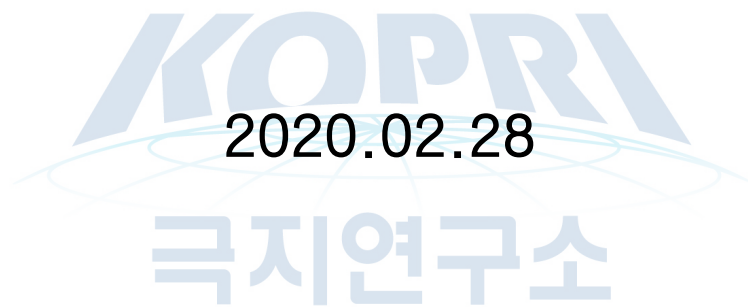


Study of the variation of the polar upper  
atmosphere caused by the energy transfer  
from space environment and lower  
atmosphere

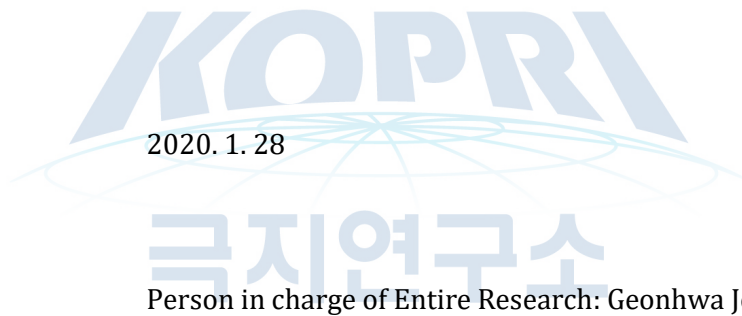


한국 해양 과학기술원  
부 설 극 지 연 구 소  
(Johns Hopkins University)

# Submission

To: Chief of Korea Polar Research Institute

This report is submitted as the final report “Study of the variation of the polar upper atmosphere caused by the energy transfer from space environment and lower atmosphere” of entrusted research “Study of the auroral characteristics and auroral effect on the polar upper atmosphere” project.



Name of Entrusted Organization: Johns Hopkins University/  
Applied Physics Laboratory

Entrusted Researcher in charge: Hyosub Kil

Participating Entrusted Researchers: Hyosub Kil

# Summary

## I. Title

Study of the auroral characteristics and auroral effect on the polar upper atmosphere

## II. Purpose and Necessity of R&D

This study aims to identify the characteristics of electron density irregularities in the ionosphere and their creation mechanisms. Ionospheric electron density irregularities which are produced by complex physical processes between neutral and charged particles affect the radio communication and navigation system. Because of their scientific and practical importance significant efforts have been made to specify and predict their behavior. Ionospheric irregularities at different latitudes are understood in terms of different physical processes, but an ambiguity exists among their boundaries. We investigate unexplored aspects of ionospheric irregularities and thermospheric phenomena that are useful for the understanding of the sources of ionospheric irregularities and dynamics

## III. Contents and Extent of R&D

We investigate the spatial structure and global distribution of irregularities and thermospheric features whose sources have not yet been identified. Ionospheric and thermospheric observations from different satellites are analyzed and ground-based observations are used to support the satellite observations. Plasma density enhancements are observed in middle latitudes, and there have been debates regarding the sources of the density enhancements. We address this question by examining the spatial structure of the density enhancements using the measurements of the electron density by the formation flight of Swarm satellites. The study of ionospheric irregularities has been focused on nighttime assuming that daytime irregularities are ignorable. However, daytime irregularities are not rare phenomena and have rich information of the dynamics of the ionosphere. We investigate the role of ionospheric dynamics in the latitudinal redistribution of irregularities during daytime. Far ultraviolet emissions are observed at night in middle latitudes, and we investigate their origin by examining their global morphology.

## IV. R&D Results

Our study for the first time has identified the spatial structure of plasma blobs, and this result provides strong evidence that the generation of plasma blobs is associated with traveling ionospheric disturbances. The irregularities detected during daytime in low latitudes are turned out to be the remnants (of fossils) of bubbles developed on the previous night. Our study first identified the temporal evolution of the latitudinal distribution of fossil bubbles and its association with the fountain effect. The anomalous far ultraviolet emissions in the thermosphere are identified to be the signatures of conjugate photoelectrons, and our study for the first time has identified the global morphology of conjugate photoelectrons.

## V. Application Plans of R&D Results

Our results provide information of the disturbances in the ionosphere and thermosphere which are closely related to 'space weather'. We plan to apply these results for the improvement of Ground Based Augmentation System (GBAS) and use for the prediction of the occurrence of bubbles and TIDs by applying a deep learning method.

# Table of Contents

Chapter 1 Introduction	4
Chapter 2 Current R&D Status in Korea and Other Nations	6
Chapter 3 R&D Implementation Contents and Results	7
3.1 Proton-All Sky Imager (PASC) calibration	7
3.2 Plasma blobs associated with medium-scale traveling ionospheric disturbances	9
3.3 Daytime evolution of equatorial plasma bubbles	10
3.4 The far ultraviolet signatures of conjugate photoelectrons seen by SSUSI	12
Chapter 4 Degree of R&D Goal Achievement and Degree of Contribution to Outside Research Institute	15
Chapter 5 Application Plans of R&D Results	16
Chapter 6 References	17



# Chapter 1. Introduction

The ionosphere and thermosphere consist of the intermingled ionized and neutral gases that coexist above  $\sim 100$  km and form the outer boundary of the Earth's atmosphere with the space environment beyond. The two components strongly interact with each other via collisions and charge exchange and are coupled with the magnetosphere above and the atmosphere below. Understanding the state of the upper atmosphere requires the understanding of the individual gases, their dynamics, electrodynamics, and their complex interactions with drivers from above and below. It is also a region of Earth's atmosphere that can influence many parts of technological systems by causing drag on orbiting satellites, altering pathways for over-the-horizon communication systems for the military and commercial aviation, and causing errors in autonomous location devices used in self-driving cars, construction, and farming equipment. Improving scientific understanding of this region of Earth's atmosphere is critical for making significant progress in the ability to specify, predict, and mitigate the effects of space weather.

The major task of this project was the investigation of the characteristics of aurora using the observations of the proton all-sky cameras that were specially designed to detect auroral emissions produced by proton precipitation, but the camera data have not yet been calibrated during the project period. The calibration algorithm was developed in April 2019, and the first calibrated data were produced in December 2019. Dr. Frank Morgan in JHU/APL who has developed the calibration algorithm is testing the validity of the calibrated data, but the testing results have not yet come out. In the meantime, we decided to address the science questions in the ionosphere and thermosphere system that have not yet been resolved. Although the science topics that we have worked on during the project period were not closely related to the objectives of the project, those topics were thought to be advantageous for publication at major journals because we have expertise on those topics.

There have been controversy regarding the source of plasma blobs in middle latitudes. The idea of the bubble-blob connection is based on the observations of bubbles and blobs at the same magnetic meridian (Huang et al., 2014; Le et al., 2003; Martinis et al., 2009; Park et al., 2003, Yokoyama et al., 2007) and a certain level of similarity in the distributions of bubbles and blobs (Huang et al., 2014; Park et al., 2008). Numerical simulations have also shown the formation of blobs when bubbles develop (Krall et al., 2010a, 2010b). However, the detection of blobs in the absence of bubbles indicates that bubbles are not a prerequisite for the development of blobs (Kil et al., 2011, 2015). The idea of the medium-scale traveling ionospheric disturbance (MSTID)-blob connection is supported by the observations of blobs at the locations of MSTIDs (Kil & Paxton, 2017; Miller et al., 2014) and some similarities in the occurrence climatology of blobs and MSTIDs (Choi et al., 2012; Haaser et al., 2012). Our study addresses the origin of plasma blobs using the observations of the formation flight of Swarm satellites.

Nighttime bubbles in the equatorial region have been observed by various techniques. They appear as plasma depletions in in situ measurements (e.g. Kil et al., 2009; Abdu et al., 2012; Martinis et al., 2003; Hysell et al., 2005; Kudeki & Bhattacharyya, 1999; Tsunoda, 1983; Yokoyama et al., 2011). However, little is known about daytime bubble signatures. One reason may be that bubble signatures are difficult to detect during daytime. Optical observations are not usable for the detection of daytime bubbles because the airglow during daytime is dominated by Rayleigh scattering of sunlight by the troposphere that is thousands of times brighter than the ionospheric signal. Fossils of nighttime bubbles in the topside are not detectable during the day by ionosondes on the ground. Daytime backscatter echoes have been detected in the upper ionosphere by the radar at Jicamarca (Chau & Woodman, 2001; Woodman et al., 1985), but they are rare events and their connection with bubbles has not yet been verified. The daytime signatures of bubbles were

identified from the measurements of the electron density by the Communication/Navigation Outage Forecasting System (C/NOFS) satellite. Huang et al. (2013) reported several events of daytime irregularities associated with bubbles on previous nights from C/NOFS observations. This observational result indicated that the lifetime of a bubble is much longer than we usually think of it as being. However, the lifetime of a bubble would also be affected by other factors such as the plasma depletion depth, solar zenith angle, and solar activity. We do not yet have an accurate or complete knowledge of the conditions required for bubbles to persist until they can be observed on the dayside. This study reports on daytime irregularities identified from the first Republic of China satellite (ROCSAT-1) observations. Our investigation focuses on the role of ionospheric dynamics in the evolution of bubbles during daytime.

Photoionization of neutral particles on the sunlit side of the atmosphere produces suprathermal electrons whose energy is greater than that of ambient, thermalized, electrons. These suprathermal electrons on the sunlit side flow into the nightside along the magnetic field lines and lose their energy through collisions with neutral particles and plasma at the local region. "Conjugate photoelectrons" represent those suprathermal electrons that have traveled from the magnetic conjugate locations. Conjugate photoelectrons are manifested by the observations of electron temperature enhancement at predawn by radars (Carlson, 1966; Evans, 1967; Evans & Gastman, 1970) and satellites (Kakinami et al., 2010; Oyama et al., 1996), observations of airglow at visual (Bennett, 1969; Carlson & Suzuki, 1974; Christensen, 1975; Duboin et al., 1968; Shepherd et al., 2014) and far ultraviolet (FUV) (Buckley & Moos, 1971; Meier, 1971) wavelengths, and simultaneous in situ rocket measurements of airglow, electron density and temperature, and photoelectron flux (Shepherd et al., 1978). A variety of methods have been used to model the generation, transport, and impact of photoelectrons (Varney et al., 2012, and references therein). As the references cited above show, there has been relatively little work on the subject of conjugate photoelectrons recently. Our study for the first time derive the global morphology of conjugate photoelectrons by analyzing the measurements of oxygen atom (OI) 130.4 nm emission by the Special Sensor Ultraviolet Spectrographic Imager (SSUSI).

## Chapter 2. Current R&D Status in Korea and Other Nations

As well as scientific importance as a natural laboratory for the study of plasma instabilities and plasma-neutral interaction, the practical importance of the Earth's ionosphere and thermosphere is increasing with the development of technology. The changes of the ionosphere and thermosphere directly impact the tracking of satellite orbits, satellite lifetime, radio communication, navigation system, and power lines on the ground. Because space weather affects every day lives of the modern society, significant efforts have been made to predict or forecast space conditions.

Currently, USA is most advanced in these fields by the number of scientists, knowledge, and research fund. The USA has been participating in the study of space phenomena from equatorial region to polar region and in all longitudes by operating various satellite and ground-based observational facilities. The USA is also hosting important space related meetings (e.g., American Geophysical Union meetings, space weather workshop) and journals. Two notable recent trends are to develop models that unite the physical processes at lower atmosphere, upper atmosphere and ionosphere, and magnetosphere and to make simultaneous observations worldwide by using constellation of satellites. Japan has long been interested in space science. Japan has been deploying ground-based observational facilities worldwide to collect data and developing ionosphere, thermosphere, and magnetosphere models. The level of European Union may be similar to Japan. These are big three in space science. China is rapidly growing in this field by increasing ground-based observational facilities. Taiwan started exploration of space earlier than Korea. Taiwan successfully operated satellite mission in 1999-2004 and keep launching science mission satellites independently and also in collaboration with the USA. Brazil, Peru, and countries in Africa have been providing important observational data and the scientists in those countries are actively participating in international collaboration. However, their interests are mostly limited to the phenomena in low and middle latitudes (plasma bubble and traveling ionospheric disturbance) because of their geophysical locations. Asian countries such as Indonesia, Malaysia, Philippine, and Vietnam started paying attention on space weather recently and sending students to other countries including Korea.

The number of space scientists in Korea has been growing rapidly during the last 10 years. Current status of Korea in the field of space science may be a little bit lower level than Taiwan and China. Taiwan advances Korea in satellite mission and China advances Korea in the number of scientists and publication. KOPRI established important observational facilities in the polar region that can be comparable to those of other advanced countries. They are KOPRI's great asset for the collaborative polar research with other countries. NASA is preparing Global Dynamics Constellation (GDC) mission planning to launch multiple satellites in 2027. The key science objective of the GDC mission is to understanding the dynamics and energy deposition in the polar region. Ground-based observations are essential for the success of the GDC mission for the validation of the satellite measurements and to complement the gaps in satellite observations. By combining expertise in KASI and universities in Korea with KOPRI's assets, Korea's participation to NASA's GDC mission will provide a great opportunity for KOPRI (or Korea) to one step advance in the field of space science.

## Chapter 3. R&D Implementation Contents and Results

### 3.1 Proton-All Sky Imager (PASC) calibration

The Proton All-Sky Imager uses a tilting narrow band filter to image proton aurora H-alpha emission spectra. The filter's peak transmission wavelength is maximum at normal incidence, and decreases with increasing angle of incidence. Tilting the filter through a range of angles provides a spectrum across multiple wavelengths.

The optical design is such that light imaged at a particular pixel is collimated at the filter location. However, the filter incidence angle varies over the field of view, so different pixels see different peak wavelengths in general during an exposure while the filter is fixed at a particular angle. Post-processing is needed in order to form an image for a fixed wavelength across the field of view, or to derive a spectrum at a given pixel from a filter scan.

Imager calibration is analyzed to map peak filter transmission wavelength as a function of pixel position and filter angle. During calibration at KHO, imagers were acquired at multiple filter angles at each of four monochromatic wavelengths. Illumination was provided by an integrating sphere fed by a monochromator. Images were acquired at wavelengths 6506.21, 6544.37, 6561.47, and 6585.16 Angstroms. At each wavelength, a series of images was acquired at filter angle steps of 2°, covering a range sufficient to identify a peak in the intensity vs. filter angle curve at each pixel.

The data is processed by measuring the peak transmission filter angle for each wavelength, for each pixel independently. Plotting peak angle vs. wavelength yields a curve which is parameterized in terms of a near-normal wavelength,  $\lambda_N$ , (close to the normal incidence peak transmission wavelength), the near-normal angle  $\theta_N$  (the filter tilt angle where light imaged at the pixel is near normal incidence), and quadratic coefficients for the curve

$$\theta - \theta_N = c_0 + c_1(\lambda_N - \lambda) + c_2(\lambda_N - \lambda)^2$$

where  $\theta$  and  $\lambda$  are the peak filter angle and peak transmission wavelength at that angle respectively. A typical pixel shows a peak filter angle vs. wavelength curve like Figure 3.1.1.

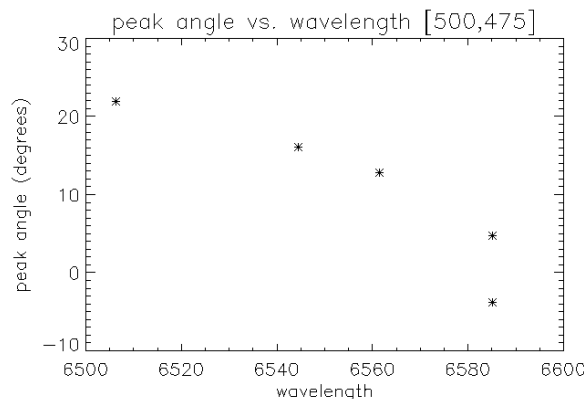


**Figure 3.1.1.** Peak filter angle vs. wavelength at pixel [500,475].

After obtaining these parameters independently at each pixel, their variation over the FOV is parameterized. The following relationships are derived.

For near-normal angle, variation across y-pixel is negligible. Variation in x is well approximated by a two-zone linear model:

$$\theta_N = 7.518 - 0.01453x, x < 460.69$$

$$\theta_N = 4.755 - 0.00853x, x > 460.69$$

Near-normal wavelength varies quadratically across  $y$ , and the peak position and magnitude both vary linearly in  $x$ , with the following parameterization:

$$\lambda_{N,max} = 6594.75 + 3.85 \times 10^{-3}x$$

$$y_{N,max} = 478.2 + 0.0137x$$

$$\lambda_N = \lambda_{N,max} - 5.2 \times 10^{-5}(y - y_{N,max})^2$$

The quadratic parameters are parameterized with:

$$c_0 = 0$$

$$c_1 = 0.50 - 1.983 \times 10^{-4}x$$

$$c_2 = -0.002186 + 7.678 \times 10^{-7}x - 2.7 \times 10^{-9}(y - 495)^2$$

One of the difficulties in the analysis of the observations is the change of the auroral structure with time and space. To minimize the effect of the spatial factor, we have chosen the observations that show stable structure during one scan period. The raw images obtained on January 9 2018 at LYB are shown in Figure 3.1.2. The images were obtained for different tilt angles. Because the time interval at each tilting step is 20 s, the observation time of each image is different. Using the data during one set of tilting operation, our task is to rebuild maps for each wavelength. Here the assumption is the aurora is stable during that period. Figure 3.1.3 shows the resulting images obtained after calibration. The final step is to derive line profiles as a function of wavelength from those images. For a given pixel, we can obtain a line profile by plotting the intensity data at different wavelengths. Figure 3.1.4 shows piles of line profiles at the region where the brightness is above 5000 ADU.

Unfortunately, we have not yet finished the validation of the line profiles. A few issues have not yet been resolved. Unexpected emission bands should be removed, the spatial variation of auroral structure should be taken into account, and the effect of emissions produced by electrons on our observation should also be clarified. APL will closely work with KOPRI to address these issues.

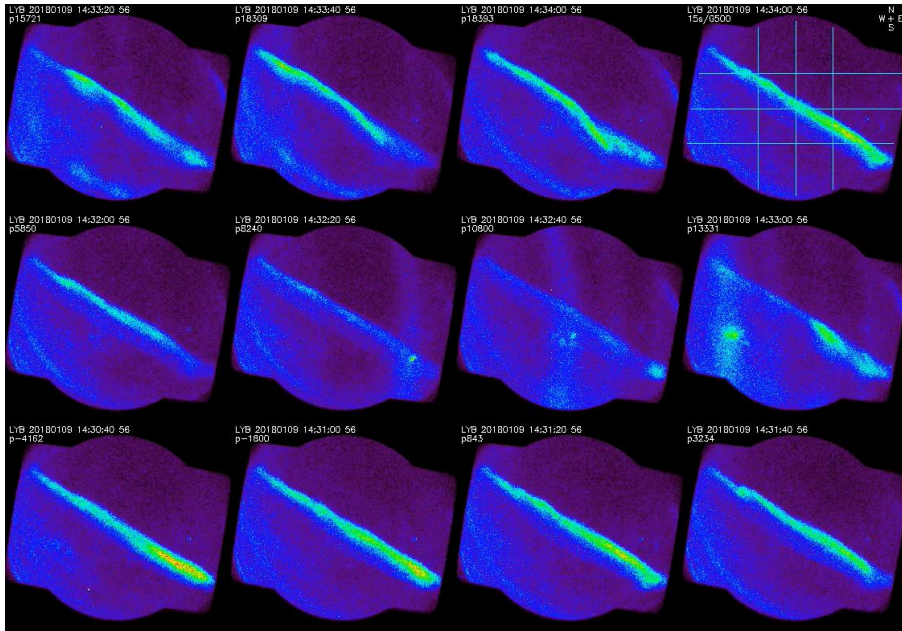


**Figure 3.1.2.** Raw images of scan 130 on January 9 2018.

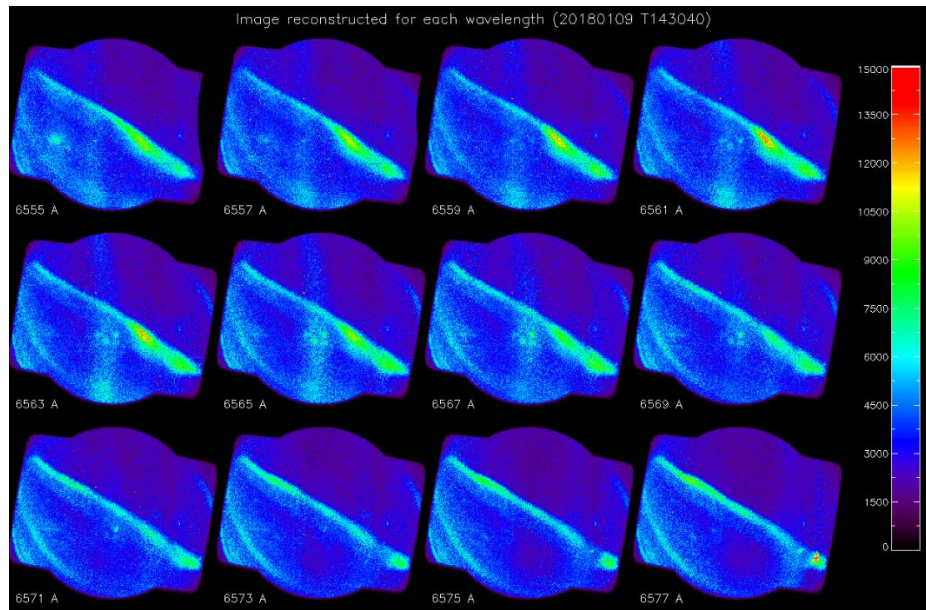


**Figure 3.1.3.** Calibrated images of the data in Figure 3.1.2.

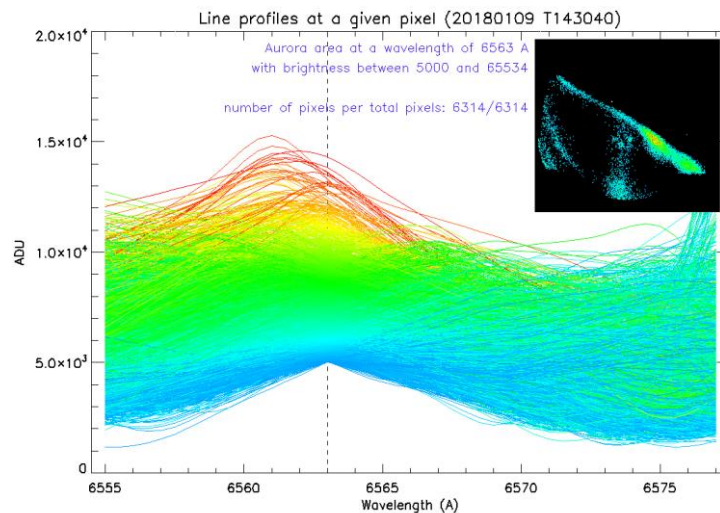


**Figure 3.1.4.** Line profiles obtained using the images whose brightness is above 5000 ADU.

### 3.2 Plasma blobs associated with medium-scale traveling ionospheric disturbances

Plasma blobs represent plasma density enhancements with respect to ambient plasma. The formation of blobs in low and middle latitudes is understood in association with either equatorial plasma bubbles or medium scale traveling ionospheric disturbances (MSTIDs). This study reports blob events identified from the Swarm satellite observations in 2014. Those blobs show the conjugate property and the alignment in the northwest-southeast direction in the Northern Hemisphere and southwest-northeast direction in the Southern Hemisphere. These are the typical characteristics of nighttime MSTIDs. The observation of MSTIDs in the total electron content maps and the absence of bubbles in the equatorial region at the times of the blob detection further support the association of those blobs with MSTIDs.

Figure 3.2.1a shows the measurements of the electron density by Swarm-A and -C on 11 February 2014. Swarm orbits are shown in Figure 1b. The locations of blobs are indicated by horizontal black bars in the density plots and vertical black bars in Swarm orbit plots. In Figure 1a, the locations of blobs are symmetric with respect to the magnetic equator. Note the alignment direction of the blobs in Figure 1b. By connecting blobs A and C in the Northern hemisphere we can identify their alignment in the northwest-southeast direction. Blobs B and D in the Southern Hemisphere are aligned in the southwest-northeast direction. These alignments along with the conjugate property are the typical characteristics of nighttime MSTIDs (Martinis et al., 2011; Otsuka et al., 2004; Saito et al., 2001). The total electron content (TEC) perturbation maps, produced by subtracting the 1-h running average, are shown for 22:20 UT and 22:50 UT in Figure 1c. Wave-like TEC modulations are not obvious in the TEC perturbation maps. However, we can trace the southwestward movement of the TEC enhancement (black circle) with time by comparing the two maps. If the TEC enhancement extends to the northwest direction following the typical MSTID alignment, this matches the locations of blobs A and C.

Similar spatial alignments of blobs are identified from a few other blob events, and these observations provide strong evidence that the development of blobs from MSTIDs. The detection of MSTIDs by TEC perturbation maps near the locations of the blobs and the absence of bubbles in the equatorial region at the times of the blob detection further support the association of those blobs with MSTIDs. However, we do not know yet to what extent the creation of blobs can be attributed to MSTIDs and under what conditions blobs develop from MSTIDs. Statistical analysis of the characteristics of blobs and numerical simulations of MSTIDs under various ionosphere/thermosphere conditions are necessary to address these questions.

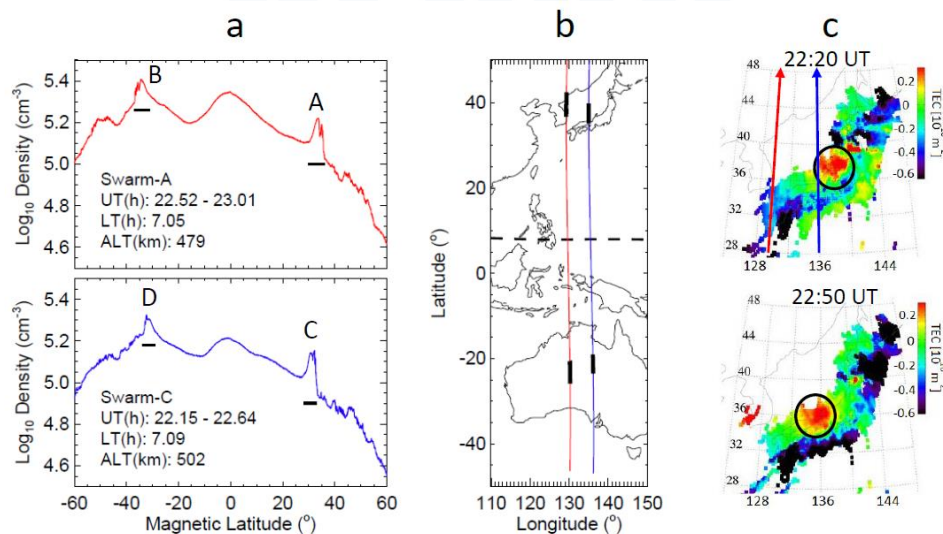


**Figure 3.2.1** (a) Swarm-A and Swarm-C observations of the electron density on 11 February 2014. The observations were made around 7.0 h LT. The locations of blobs are indicated by black horizontal bars. (b) Swarm-A (red) and Swarm-C (blue) orbits with the detection locations of blobs (black lines). The black dashed line indicates the magnetic equator. (c) TEC perturbation maps for at 22:20 and 22:50 UT with Swarm-A and Swarm-C orbits by red and blue arrows, respectively. Black circles indicate the TEC enhancements that might be related to blobs A and C.

### 3.3 Daytime evolution of equatorial plasma bubbles

Plasma bubbles in the equatorial F region are thought of as nighttime phenomena because they develop at night and are assumed to vanish after sunrise. However, bubbles occasionally persist throughout the night and into the day. This study investigates the origin of daytime irregularities and their evolution using data from the first Republic of China satellite (ROCSAT-1). Our results

show that daytime irregularities occur in the longitudes where bubbles have developed on previous nights. A newly reported feature is the observation of the temporal variation of the locations of daytime irregularities; daytime irregularities are concentrated near the magnetic equator early in the morning, but the location gradually shifts to higher latitudes with time. This phenomenon is explained in terms of the latitudinal redistribution of fossil bubbles by the ionospheric fountain effect.

Daytime irregularities show various morphologies. Some irregularities, specially the irregularities detected in the morning sector, maintain the bubble morphology (plasma depletions), but in many cases daytime irregularities show irregular fluctuations. We have traced the history of fifty events of daytime irregularities using the method shown in Figure 3.3.1. The association of daytime irregularities with bubbles on the previous night was identified for the majority of the daytime irregularity events. This investigation result indicates that daytime irregularities in low latitudes can be interpreted to be fossils of nighttime bubbles.

From many daytime irregularity events we have noticed the occurrence of daytime irregularities outside of the magnetic equator. To verify this property, the latitudinal distribution of the irregularities is derived using all ROCSAT-1 data acquired from March 1999 to June 2004. Figure 3.3.2a shows the occurrence probability of the irregularities as a function of LT and magnetic latitude. We examine the temporal variation of the occurrence rate from the evening in order to track the evolution of bubbles from the development. The occurrence rate abruptly increases from near zero to 20% at 19 hr LT in the equatorial region. This observation is consistent with our understanding of the development of bubbles just after sunset. The peak of the occurrence rate appears around 22 hr LT. From the figure we can identify the increasing latitudinal extension of the locations of the irregularities with time during 19–22 hr LT. This phenomenon is expected to be arising from the growth of bubbles during that time period. The retraction of the irregularity locations to the equatorial region after midnight may be explained by the decay of the bubbles and the downward motion of the ionosphere at night. The occurrence rate rapidly decreases after around 6–7 hr LT (or after sunrise) due to the filling of the bubbles by the photoionization of oxygen atoms. However, the decrease of the occurrence rate at the sunrise terminator is not as dramatic as the rapid increase of the occurrence rate at the sunset terminator. The relatively gradual decrease of the occurrence rate at the sunrise terminator may indicate that some portion of the topside signature of nighttime bubbles could survive after sunrise. In Figure 3.3.2a, irregularities are not confined to low latitudes at night. Traveling ionospheric disturbances (TIDs) are considered to be important sources of the irregularities beyond low latitudes, but the latitudinal boundary of the irregularities associated with bubbles and TIDs is not distinguishable from the observational data.

The occurrence rate of the irregularities during daytime is a few times smaller than that of the irregularities at night. An interesting feature in the distribution of the irregularities during daytime is the temporal variation of the irregularity location. Figure 3.3.2b is the enlarged image of the red box in Figure 3.3.2a using a different color scale. Irregularities are concentrated within  $\pm 10^\circ$  magnetic latitudes in the morning. The concentration location gradually moves to higher latitudes in both hemispheres as time progresses, and the concentration peak appears around  $\pm 15^\circ$  magnetic latitudes in the afternoon. This phenomenon has not yet been reported. This phenomenon is considered to indicate the involvement of ionospheric dynamics in the evolution of bubbles during daytime. This phenomenon is consistent with the transport of the ambient plasma driven by the fountain effect. Numerical simulations are necessary to identify the effect of the ionospheric dynamics on the evolution (or distribution) of bubbles and the factors that affect the lifetime of a bubble.

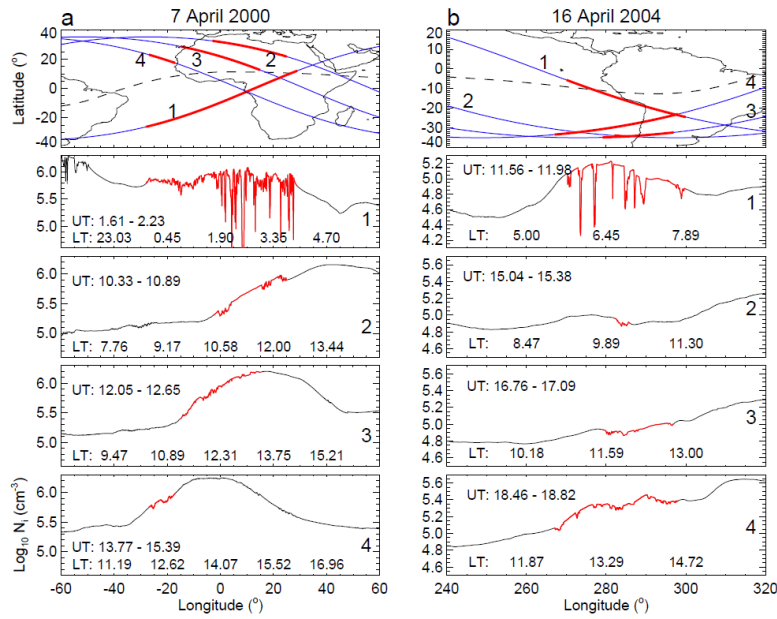


**Figure 3.3.1.** Series of ROCSAT-1 observations on (a) 7 April 2000 and (b) 16 April 2004. The detection locations of bubbles at night and daytime irregularities are indicated in red on the ROCSAT-1 orbit tracks and density measurements. The black dashed lines in top panels indicate the magnetic equator.

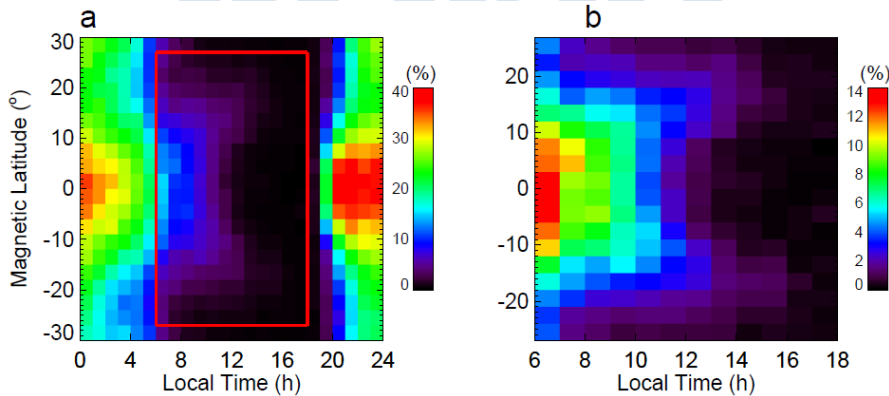


**Figure 3.3.2.** (a) Distribution of the irregularities obtained using the threshold  $S > 0.002$ . (b) Enlarged image of the red box in Figure 4a. Note the change in the color bar scale of a factor of 3. The distribution is derived using all ROCSAT-1 data acquired from March 1999 to June 2004. The occurrence probability is determined by the ratio of the number of orbits with irregularities to the total number of orbits.

### 3.4 The far ultraviolet signatures of conjugate photoelectrons seen by SSUSI

This study investigates the origin of anomalous far ultraviolet emissions observed at night at the subauroral region by the Special Sensor Ultraviolet Spectrographic Imager (SSUSI) on board the Defense Meteorological Satellite System (DMSP)-F16 satellite. The global distribution of the anomalous emission is derived using the measurements of the oxygen atom 130.4 nm emission in 2017. Our results show the extension of the anomalous emission from high latitudes to middle

latitudes in the Northern American-Atlantic sector during the December solstice and in the Southern Australia-New Zealand sector during the June solstice. These observations indicate that the anomalous emission occurs in the winter hemisphere and is pronounced at locations close to the magnetic poles. The good agreement between the morphology of the anomalous emission and the predicted distribution of conjugate photoelectrons leads to the conclusion that the anomalous emissions are the signatures of conjugate photoelectrons.

The global behavior of the anomalous OI emission is investigated using the maps of OI 130.4 nm intensity derived using the DMSP-F16/SSUSI data in 2017. Figures 3.4.1c and 2.3.1d show the maps in solstices. To explain the morphology of the anomalous emissions, the geomagnetic field lines and the solar zenith angle (SZA) derived using different methods are shown in Figures 3.4.1a and 3.4.1b. We first explain the blue lines in Figure 3.4.1a. The straight blue line in the Southern (summer) Hemisphere indicates  $100^\circ$  SZA at 4.0 hr local solar time (LST). The blue line in the Northern (winter) Hemisphere is its magnetic conjugate location.  $100^\circ$  SZA corresponds to the sunset time near an altitude of 100 km. This is a conservative boundary; sunset effectively occurs at earlier times (lower SZA) for the wavelengths of sunlight that create ionization due to the wavelength dependent attenuation of sunlight along the line-of-sight from the Sun to the point in the atmosphere under consideration. Because photoelectrons exist poleward of the blue line in the Southern Hemisphere and these photoelectrons can travel to the Northern Hemisphere along the magnetic field lines, the blue line in the Northern Hemisphere represents the latitudinal boundary of conjugate photoelectrons. We have chosen 4.0 hr LST for the conjugate calculation to match the LST of the SSUSI observation in the Northern Hemisphere. The same method is used for the blue lines in Figure 3.4.1b. In the June solstice, the latitude of the  $100^\circ$  SZA and its conjugate locations are calculated for 3.25 hr LST to match the LST of the SSUSI observation in the Southern Hemisphere. The blue lines in the winter hemisphere are shown in Figures 3.4.1c and 3.4.1d. The large-scale morphology of the anomalous emission is represented by the blue lines, but significant deviations also exist.

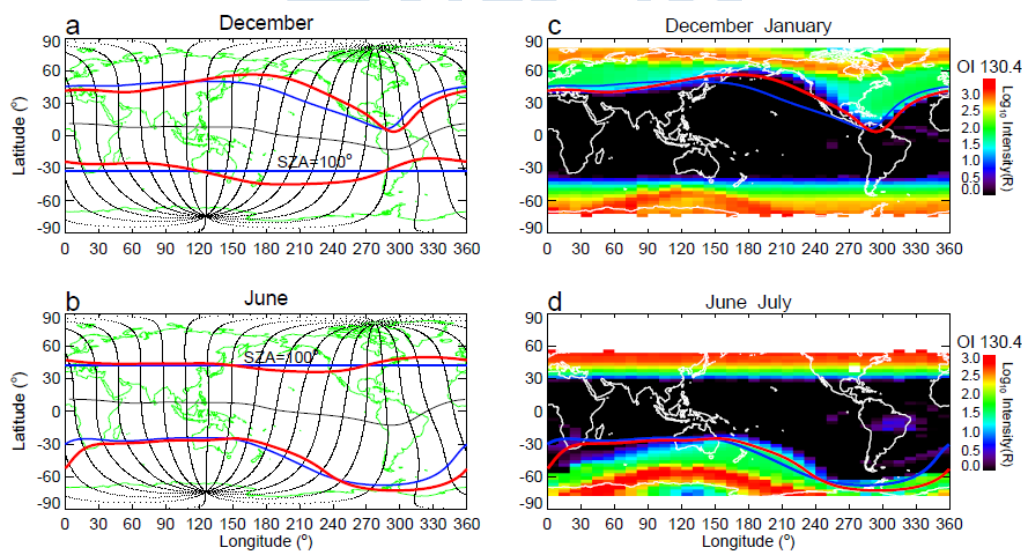


**Figure 3.4.1.** (a and b) Earth's magnetic field configuration and magnetic conjugacy in 22 December and 22 June. The blue and red lines in the summer hemisphere indicate the locations of  $100^\circ$  SZA calculated using two different methods. Their magnetic conjugate locations are shown by the same color. See the text for the details of the blue and red lines. (c and d) SSUSI OI 130.4 maps in December-January and June-July with the conjugate SZA lines shown in Figure 3.4.1a and 3.4.1b.

The blue lines assume that photoelectrons are produced at the same LST (4 hr in the December solstice and 3.25 hr in the June solstice) at all longitudes in the summer hemisphere and are responsible for the conjugate photoelectrons at the same LST in the winter hemisphere. This assumption is reasonably accurate for the longitudes where the magnetic declination is zero. At the longitudes where the magnetic declination is non-zero, however, conjugate photoelectrons originate from the regions of different LSTs. We explain the situations around 250°E (positive magnetic declination) and 320°E (negative magnetic declination) longitudes during the December solstice. Around 250°E, the anomalous emission at 4 hr LST in the Northern Hemisphere is produced by the photoelectrons created at an earlier time (3 hr LST) in the Southern Hemisphere. Then, we have to find the location of the 100° SZA at 3.0 hr LST instead of at 4.0 hr LST in the Southern (summer) Hemisphere. Because the latitude of 100° SZA is the highest at midnight and moves to lower latitudes as a function of time relative to midnight, the location of 100° SZA at 3.0 hr LST is at a higher latitude than that at 4.0 hr LST. The opposite situation occurs at 320°E; the photoelectrons produced at 5.0 hr LST in the Southern Hemisphere are responsible for the anomalous emission detected at 4.0 hr LST in the Northern Hemisphere. The location of 100° SZA at 5.0 hr LST is at a lower latitude than that at 4.0 hr LST. In Figure 3.4.1a, the red line in the Southern Hemisphere shows the corrected 100° SZA after taking care of the magnetic declination effect. The red lines in Figure 3.4.1b are obtained using the same method for 40°S reference latitude and 3.25 hr LST. Depending on the magnetic field configuration, the locations of 100° SZA and its conjugate locations shift to higher or lower latitudes relative to the blue line. This variation is consistent with our explanation of the dependence of the latitude of 100° SZA on the magnetic declination. In Figures 3.4.1c and 3.4.1d, the morphology of the anomalous emission is represented better after taking into account the magnetic declination effect (red lines).

This study demonstrates that the observations of FUV emissions from space are valuable resources for the study of conjugate photoelectrons. The FUV emissions produced by conjugate photoelectrons are the consequence of the production of photoelectrons in the sunlit side, their interhemispheric transport, and their impact on the conjugate atmosphere. These processes are sensitive to the solar flux, the density, velocity, composition, and temperature of neutral and charged particles. The behavior of conjugate photoelectrons during magnetically disturbed periods is expected to be different from that during magnetically quiet periods because of the changes in the ionospheric and thermospheric conditions. The interhemispheric photoelectron flow through the magnetosphere and thermosphere will also be affected by geomagnetic disturbances. The FUV observations by SSUSI and GUVI can be used for the validation of these physical processes.

## Chapter 4. Degree of R&D Goal Achievement and Degree of Contribution to Outside Research Institute

We have published three research papers at the journal 'Geophysical Research Letters' under the support of the KOPRI project. Because the journal accepts the papers whose ideas or discoveries are worth prompt publication, the scientific value of our papers has already been recognized. Our study of plasma blobs showed how to use the observations of formation flight for the study of spatial structures of the ionosphere. Planners of mission concepts will be interest in our results. We demonstrated that plasma bubbles could survive throughout the day and be transported to beyond equatorial region by the fountain effect. Researchers of the evolution of bubbles and ionospheric dynamics would be interested in these results. We first identified the global morphology of conjugate photoelectrons. This result will provide a valuable reference when people validate the signatures of conjugate photoelectrons in the ionosphere and thermosphere.

As we proposed, we have published three papers at the top level journal and had a KOPRI scientist (Dr. Geonhwan Jee) as a coauthor. On that aspect, we achieved the goal. We have not yet made a publication with the observations of the proton all-sky imager because the calibration of the instrument was made very recently. Although the project has ended 2019, the analysis of the observation data will be continued in collaboration with KOPRI.

### **Publications**

Kil, H., R. K. Schaefer, L. J. Paxton, and G. Jee (2020), The far ultraviolet signatures of conjugate photoelectrons seen by the Special Sensor Ultraviolet Spectrographic Imager, *Gephys. Res. Lett.*, <https://doi.org/10.1029/2019GL086383>.

Kil, H., L. J. Paxton, W. K. Lee, and G. Jee (2019), Daytime evolution of equatorial plasma bubbles observed by the first Republic of China Satellite, *Gephys. Res. Lett.*, 46, 5028-5027. <https://doi.org/10.1029/2019GL082903>.

Kil, H., L. J. Paxton, G. Jee, and R. Nikoukar (2019), Plasma blobs associated with medium-scale traveling ionospheric disturbances, *Gephys. Res. Lett.*, 46, 3575-3581. <https://doi.org/10.1029/2019GL082026>.

## Chapter 5. Application Plans of R&D Results

Our results and database have rich information of the electron density structures in the ionosphere that are useful for the study of plasma instabilities and radio scintillation. We will extend our investigation to the studies of the interaction of bubbles and MSTIDs, daytime MSTIDs, and the effect of conjugate photoelectron on the triggering of plasma instabilities. We plan to develop a prediction model of bubbles and MSTIDs by applying a deep learning method. For this purpose, we will produce the database of irregularities by combining the results obtained from all available satellite data. Aircraft use their height information from Ground Based Augmentation System (GBAS) when they land. GBAS provides height information using the measurements of the electron density (or time delay) at nearby GPS stations. When the spatial gradient of the electron density is significant, the actual height of aircraft and the height provided by GBAS can be significant. In that situation, aircraft cannot use GBAS. Because the spatial gradient in electron density is produced by ionospheric structures such as bubbles and TIDs, accurate knowledge of bubbles and TIDs is essential to maximize the use of GBAS or give a warning message to aircraft. The ultimate goal of our study of irregularities is to apply irregularity information for practical purposes. At this stage, we cannot specify the application of the observational results of proton all-sky imagers because the validation of the results have not yet been finished.



## Chapter 6 References

- Abdu, M. A., Batista, I. S., Reinisch, B. W., MacDougall, J. W., Kherani, E. A., & Sobral, J. H. A. (2012). Equatorial range spread F echoes from coherent backscatter, and irregularity growth processes, from conjugate point digital ionograms. *Radio Science*, 47, RS6003. <https://doi.org/10.1029/2012RS005002>
- Buckley, J. L., & Moos, H. W. (1971). Vacuum ultraviolet spectra of the late twilight airglow. *Journal of Geophysical Research*, 76(34). <https://doi.org/10.1029/JA076i034p08378>
- Carlson, H. C. (1966). Ionospheric heating by magnetic conjugate-point photoelectrons. *Journal of Geophysical Research*, 71(1). <https://doi.org/10.1029/JZ071i001p00195>
- Carlson, R. W., & Suzuki, K. (1974). Observation of  $O^+$  ( ${}^2P_o - {}^2D_o$ )  $\lambda$  7319 Å emission in the twilight and night airglow. *Nature*, 248, 400–401. <https://doi.org/10.1038/248400a0>
- Chau, J. L., & Woodman, R. F. (2001). Interferometric and dual beam observations of daytime spread-F-like irregularities over Jicamarca. *Geophysical Research Letters*, 28, 3581–3584. <https://doi.org/10.1029/2001GL013404>
- Choi, H.-S., Kil, H., Kwak, Y.-S., Park, Y.-D., & Cho, K.-S. (2012). Comparison of the bubble and blob distributions during the solar minimum. *Journal of Geophysical Research*, 117, A04314. <https://doi.org/10.1029/2011JA017292>
- Christensen, A. B. (1975). Observations of OI 7774 emission excited by conjugate photoelectrons. *Planetary and Space Science*, 23, 831–842. [https://doi.org/10.1016/0032-0633\(75\)90020-3](https://doi.org/10.1016/0032-0633(75)90020-3)
- Duboin, M.-L., Lejeune, G., Petit, M., & Weill G. (1968). Excitation of oxygen ion lines and ionospheric heating by conjugate photoelectrons. *Journal of Atmospheric Terrestrial Physics*, 30, 299–304. [https://doi.org/10.1016/0021-9196\(68\)90084-6](https://doi.org/10.1016/0021-9196(68)90084-6)
- Evans, J. V. (1967). Midlatitude electron and ion temperatures at sunspot minimum. *Planetary and Space Science*, 15, 1557–1570. [https://doi.org/10.1016/0032-0633\(67\)90089-X](https://doi.org/10.1016/0032-0633(67)90089-X)
- Evans, J. V., & Gastman, I. J. (1970). Detection of conjugate photoelectrons at Millstone Hill. *Journal of Geophysical Research*, 75(2). <https://doi.org/10.1029/JA075i004p00807>
- Haaser, R. A., Earle, G. D., Heelis, R. A., Klenzing, J., Stoneback, R., Coley, W. R., & Burrell, A. G. (2012). Characteristics of low-latitude ionospheric depletions and enhancements during solar minimum. *Journal of Geophysical Research*, 117, A10305. <https://doi.org/10.1029/2012JA017814>
- Huang, C.-S., Le, G., de La Beaujardiere, O., Roddy, P. A., Hunton, D. E., Pfaff, R. F., & Hairston, M. R. (2014). Relationship between plasma bubbles and density enhancements: Observations and interpretation. *Journal of Geophysical Research: Space Physics*, 119, 1325–1336. <https://doi.org/10.1002/2013JA019579>
- Huang, C.-S., de La Beaujardiere, O., Roddy, P. A., Hunton, D. E., Ballenthin, J. O., & Hairston, M. R. (2013). Long-lasting daytime equatorial plasma bubbles observed by the C/NOFS satellite. *Journal of Geophysical Research: Space Physics*, 118, 2398–2408. <https://doi.org/10.1002/jgra.50252>
- Hysell, D. L., Larsen, M. F., Swenson, C. M., Barjatya, A., Wheeler, T. F., Sarango, M. F., et al. (2005). Onset conditions for equatorial spread F determined during EQUIS II. *Geophysical Research Letters*, 32, L24104. <https://doi.org/10.1029/2005GL024743>
- Kakinami, Y., Balan, N., Liu, J. Y., & Oyama, K.-I. (2010). Predawn ionospheric heating observed by Hinotori satellite. *Journal of Geophysical Research*, 115, A01304. <https://doi.org/10.1029/2009JA014334>
- Kil, H., Paxton, L. J., & Oh, S.-J. (2009). Global bubble distribution seen from ROCSAT-1 and its association with the pre-reversal enhancement. *Journal of Geophysical Research*, 114, A06307. <https://doi.org/10.1029/2008JA013672>
- Kil, H., & Paxton, L. J. (2017). Global distribution of nighttime medium-scale traveling ionospheric disturbances seen by Swarm satellites. *Geophysical Research Letters*, 44, 9176–9182. <https://doi.org/10.1002/2017GL074750>

- Kil, H., Choi, H.-S., Heelis, R. A., Paxton, L. J., Coley, W. R., & Miller, E. S. (2011). Onset conditions of bubbles and blobs: A case study on 2 March 2009. *Gephysical Research Letters*, *38*, L06101. <https://doi.org/10.1029/2011GL046885>
- Kil, H., Kwak, Y.-S., Lee, W. K., Miller, E. S., Oh, S.-J., & Choi, H.-S. (2015). The causal relationship between plasma bubbles and blobs in the low-latitude F region. *Journal of Geophysical Research*, *120*, 3961–3969. <https://doi.org/doi:10.1002/2014JA020847>
- Krall, J., Huba, J. D., Joyce, G., & Yokoyama, T. (2010a). Density enhancements associated with equatorial spread F. *Annales Geophysicae*, *28*, 327–337. <https://doi.org/10.5194/angeo-28-327-2010>
- Krall, J., Huba, J. D., Ossakow, S. L., & Joyce, G. (2010b). Equatorial spread F fossil plumes. *Annales Geophysicae*, *28*, 2059–2069. <https://doi.org/10.5194/angeo-28-2059-2010>
- Kudeki, E., & Bhattacharyya, S. (1999). Postsunset vortex in equatorial F-region plasma drifts and implications for bottomside spread F. *Journal of Geophysical Research*, *104*(A12), 28,163–28,170. <https://doi.org/10.1029/1998JA900111>
- Le, G., Huang, C.-S., Pfaff, R. F., Su, S.-Y., Yeh, H.-C., Heelis, R. A., et al. (2003). Plasma density enhancements associated with equatorial spread F: ROCSAT-1 and DMSP observations. *Journal of Geophysical Research*, *108*(A8), 1318. <https://doi.org/doi:10.1029/2002JA009592>
- Martinis, C., Eccles, J. V., Baumgardner, J., Manzano, J., & Mendillo, M. (2003). Latitude dependence of zonal plasma drifts obtained from dual-site airglow observations. *Journal of Geophysical Research*, *108*(A3), 1129. <https://doi.org/10.1029/2002JA009462>
- Martinis, C., Baumgardner, J., Wroten, J., & Mendillo, M. (2011). All-sky imaging observations of conjugate medium-scale traveling ionospheric disturbances in the American sector. *Journal of Geophysical Research*, *116*, A05326. <https://doi.org/10.1029/2010JA016264>
- Martinis, C., Baumgardner, J., Mendillo, M., Su, S.-Y., & Aponte, N. (2009). Brightening of 630.0 nm equatorial spread-F airglow depletions. *Journal of Geophysical Research*, *114*, A06318. <https://doi.org/10.1029/2008JA013931>
- Meier, R., R. (1971). Observations of conjugate excitation of the O I 1304-A airglow. *Journal of Geophysical Research*, *76*(1). <https://doi.org/10.1029/JA076i001p00242>
- Miller, E. S., Kil, H., Makela, J. J., Heelis, R. A., Talaat, E. R., & Gross, A. (2014). Topside signature of medium-scale traveling ionospheric disturbances. *Annales Geophysicae*, *32*, 959–965. <https://doi.org/10.5194/angeo-32-959-2014>
- Otsuka, Y., Shiokawa, K., Ogawa, T., & Wilkinson, P. (2004). Geomagnetic conjugate observations of medium-scale traveling ionospheric disturbances at midlatitude using all-sky airglow imagers. *Gephysical Research Letters*, *31*, L15803. <https://doi.org/10.1029/2004GL020262>
- Oyama, K.-I., Balan, N., Watanabe, S., Takahashi, T., Isoda, F., Bailey, G. J., & Oya, H. (1996). Morning overshoot of Te enhanced by downward plasma drift in the equatorial topside ionosphere. *Journal of Geomagnetism and Geolectricity*, *48*. <https://doi.org/10.5636/jgg.48.959>
- Park, J., Min, K. W., Lee, J.-J., Kil, H., Kim, V. P., Kim, H.-J. et al. (2003). Plasma blob events observed by KOMPSAT-1 and DMSP F15 in the low latitude nighttime upper ionosphere. *Gephysical Research Letters*, *30*(21), 2114. <https://doi.org/10.1029/2003GL018249>
- Park, J., Min, K. W., Kim, V. P., Kil, H., Kim, H. J., Lee, J. J., et al. (2008). Statistical description of low-latitude plasma blobs as observed by DMSP F15 and KOMPSAT-1. *Advances in Space Research*, *41*, 650–654. <https://doi.org/10.1016/j.asr.2007.04.089>
- Peterson, W. K., Doering, J. P., Potemra, T. A., McEntire, R. W., & Bostrom, C. O. (1977). Conjugate photoelectron fluxes observed on Atmosphere Explorer C. *Geophysical Research Letters*, *4*, 109. <https://doi.org/10.1029/GL004i003p00109>
- Saito, A., Nishimura, M., Yamamoto, M., Fukao, S., Kubota, M., Shiokawa, K., et al. (2001). Traveling ionospheric disturbances detected in the FRONT campaign. *Gephysical Research Letters*, *28*, No.4, 689–692. <https://doi.org/10.1029/2000GL011884>
- Shepherd, G. G., Pieau, J. F., Ogawa, T., Tohmatsu, T., Oyama, K., & Watanabe Y. (1978). Direct measurement of conjugate photoelectrons and predawn 630 nm airglow. *Planetary and Space Science*, *26*, 221–217. [https://doi.org/10.1016/0032-0633\(78\)90086-7](https://doi.org/10.1016/0032-0633(78)90086-7)

- Shepherd, G. G., Cho, Y.-M., Fomichev, V. I., & Martynenko, O. V. (2014). Characteristics of the O<sup>+</sup>(2P-2D) 732.0 and 733.0nm airglow emissions observed with WINDII and simulated with the C-IAM. *Geophysical Research Letters*, 41, 5354–5360. <https://doi.org/10.1002/2014GL060840>
- Tsunoda, R. T. (1983). On the generation and growth of equatorial backscatter plumes: 2. Structuring of the west walls of upwellings. *Geophysical Research Letters*, 88(A6), 4869–4874. <https://doi.org/10.1029/10.1029/JA088iA06p04869>
- Woodman, R. F., Pingree, J. E., & Swartz, W. E. (1985). Spread-F-like irregularities observed by the Jicamarca radar during the daytime. *Journal of Atmospheric and Solar-Terrestrial Physics*, 47, 867–874. [https://doi.org/10.1016/0021-9169\(85\)90061-3](https://doi.org/10.1016/0021-9169(85)90061-3)
- Varney, R. H., Swartz, W. E., Hysell, D. L., & Huba, J. D. (2012). SAMI2-PE: A model of the ionosphere including multistream interhemispheric photoelectron transport. *Journal of Geophysical Research*, 117, A06322, <https://doi.org/10.1029/2011JA017280>
- Yokoyama, T., Su, S.-Y., & Fukao, S. (2007). Plasma blobs and irregularities concurrently observed by ROCSAT-1 and Equatorial Atmosphere Radar, *Journal of Geophysical Research*, 112, A05311. <https://doi.org/10.1029/2006JA012044>
- Yokoyama, T., Yamamoto, M., Otsuka, Y., Nishioka, M., Tsugawa, T., Watanabe, S., & Pfaff, R. F. (2011). On postmidnight low-latitude ionospheric irregularities during solar minimum: 1. Equatorial Atmosphere Radar and GPS-TEC observations in Indonesia. *Journal of Geophysical Research*, 116, A11325. <https://doi.org/10.1029/2011JA016797>



## **Warning**

- 1. This report is a report of research results of a project entrusted by the Korea Polar Research Institute.**
- 2. When you present the contents of this report, you must state that these contents are research results of a project entrusted by the Korea Polar Research Institute.**
- 3. Materials concerning the nation's classified science and technology information must not be presented or disclosed.**